



HAL
open science

Thermally Triggered Interface for Simplified Organic Solar Cells

Suwapat Kongsabay, Gilles Henri Roche, O.J. Dautel, Vinich Promarak,
Guillaume Wantz

► **To cite this version:**

Suwapat Kongsabay, Gilles Henri Roche, O.J. Dautel, Vinich Promarak, Guillaume Wantz. Thermally Triggered Interface for Simplified Organic Solar Cells. *Advanced Photonics Research*, 2024, 10.1002/adpr.202400128 . hal-04707883

HAL Id: hal-04707883

<https://hal.science/hal-04707883v1>

Submitted on 24 Sep 2024

HAL is a multi-disciplinary open access archive for the deposit and dissemination of scientific research documents, whether they are published or not. The documents may come from teaching and research institutions in France or abroad, or from public or private research centers.

L'archive ouverte pluridisciplinaire **HAL**, est destinée au dépôt et à la diffusion de documents scientifiques de niveau recherche, publiés ou non, émanant des établissements d'enseignement et de recherche français ou étrangers, des laboratoires publics ou privés.

Thermally Triggered Interface for Simplified Organic Solar Cells

Suwapat Kongsabay, Gilles Henri Roche,* Olivier Dautel, Vinich Promarak, and Guillaume Wantz*

Organic photovoltaic (OPV) cells are commonly produced by successive printing of four layers on top of a transparent conducting electrode, with the active layer sandwiched in between interlayers followed by the top electrode. Here, the simplification of OPV manufacturing without the need to coat a hole transport layer (HTL) in inverted OPV (n-i-p) is reported. To ensure the required hole selectivity, thermally triggered molecules are directly blended in the active layer during device casting. Following thermal annealing of the complete devices, organosulfur molecules self-assembled to form a hole-transporting interface between the silver top electrode and the active layer, thereby enabling working devices. Device optimization is performed by varying the concentration of these molecules and the thermal annealing conditions. The performances of the simplified devices approach those of control devices with vacuum-evaporated MoO₃ HTLs. The solar cells exhibit very encouraging thermal and photostabilities. This work opens the route to high efficiency, simplified, and low-cost organic solar cells.

interlayers are the hole transport layer (HTL) and electron transport layer (ETL) for holes and electrons, respectively, on each side of the active layer. These multi-layered devices require successive fabrication processes for coating each layer, resulting in some complexity and higher manufacturing costs. One efficient way to minimize this expense is by simplifying the device structure. An example of this is in direct architecture, where holes are collected at ITO transparent electrode and electrons at top metallic electrode. Here, self-assembled monolayers (SAMs) of organic small molecules have been successfully utilized at the transparent ITO interfaces in order to improve the OPV device's performance and/or stability.^[8–11] Furthermore, the application of SAMs requires only small amounts of material, ≈10–100 times less than conventional

interlayers, and device properties can be tuned by functionalizing the SAM molecular structure for further device performance improvements.^[11]

In the inverted architecture, Shamieh et al. reported a spontaneously formed tri-layer stack of electron-selective interlayer/active layer/hole-selective interlayer achieved by a single processing step for inverted OPVs.^[12] This work reveals that additives blended with the organic semiconductor blend P3HT:PC₆₁BM (P3HT:poly(3-hexylthiophene), PC₆₁BM: phenyl-C₆₁-butyric acid methyl ester) can segregate to form interlayers on each side of the active layer, depending on the surface energy of the additives toward the substrate. This technology could give rise to simpler fabrication of organic electronic devices with controllable interfaces. Moreover, this methodology shows potential for industrial scalability via roll-to-roll printing.^[13,14] Our study applies the same strategy for the top electrode interface to state-of-the-art, high efficiency active layer materials with SAMs designed specifically for this purpose.

Carbazole-based SAMs were first used as an HTL in perovskite solar cells and then applied to OPV technology.^[9,15] In the works of Lin and co-workers, a SAM based on Br-2PACz ([2-(3,6-dibromo-9 H-carbazol-9-yl)ethyl]phosphonic acid), was used as an efficient hole-extracting interlayer at ITO bottom electrode interface to replace the commonly used conducting polymer blend PEDOT:PSS (PEDOT: poly(3,4-ethylenedioxythiophene), PSS: polystyrene sulfonate).^[10,11] The bromine atoms allow the molecule to obtain a significantly deeper HOMO level and


1. Introduction

Organic photovoltaics (OPVs) currently achieve a promising efficiency of over 19% power conversion efficiency (PCE).^[1–7] OPVs typically comprise an active layer sandwiched between two electrodes with two interlayers. Interlayers are added for efficient charge transport and/or blocking of charge carriers. The two

S. Kongsabay, G. H. Roche, G. Wantz
University of Bordeaux
CNRS, Bordeaux INP, IMS, UMR 5218
F-33400 Talence, France
E-mail: gilles.roche@u-bordeaux.fr; guillaume.wantz@ims-bordeaux.fr

S. Kongsabay, V. Promarak
School of Molecular Science and Engineering
Vidyasirimedhi Institute of Science and Technology
Wangchan, Rayong 21210, Thailand

O. Dautel
Institut Charles Gerhardt Montpellier
Univ. Montpellier, UMR 5253, CNRS
Montpellier, France

 The ORCID identification number(s) for the author(s) of this article can be found under <https://doi.org/10.1002/adpr.202400128>.

© 2024 The Author(s). Advanced Photonics Research published by Wiley-VCH GmbH. This is an open access article under the terms of the Creative Commons Attribution License, which permits use, distribution and reproduction in any medium, provided the original work is properly cited.

DOI: 10.1002/adpr.202400128

higher LUMO which gives it good hole selectivity for charge extraction from the bulk heterojunction (BHJ).^[11]

In general, SAM molecules consist of three moieties: a head group to anchor SAM molecules onto the substrate, a spacer, typically an alkyl chain, and a terminal functional group, which determines surface properties (See **Figure 1a**).^[16–18] To design a spontaneously organized molecule, a head group should have a chemical functionality with a specific affinity for a substrate. Numerous headgroups that bind to specific metals, metal oxides, and semiconductors have been reported in the scientific literature. The most extensively studied SAMs are derived from the adsorption of alkanethiols onto transition metals (e.g., gold, silver, platinum, and palladium).^[17] Their strong affinity is thought to originate from the possibility of forming multiple bonds with metal surfaces.^[19,20] After adsorption of these molecules onto the metal surface, the attached molecules can naturally assemble into a well-ordered and packed film structure. Consequently, the well-organized organic surface generated by the terminal end of molecules defines the functionalities of the exposed interface, such as wettability and electronic activity (dipole).

The reactivity of the thiol group in thiol-based molecules must, however, be carefully considered. For example, Béthencourt and coworkers underline that if an adjacent functional group is sensitive to a thiol, various undesirable side reactions can occur (e.g., intramolecular cyclization or intermolecular polymer formation).^[21] Especially when the thiol encounters basic conditions, it can be deprotonated and become thiolate, which acts as a strong nucleophile. These sulfur nucleophiles tend to readily react with typical electrophiles (such as alkyl halides), which can be found in common organic materials used for the active layer in OPV. This is also the case for the materials used in this study, PTQ10 (PTQ10: Poly[(thiophene)-alt-(6,7-difluoro-2-(2-hexyldecyloxy)quinoxaline)]) and Y6 (Y6: (2,2'-[[12,13-Bis(2-ethylhexyl)-12,13-dihydro-3,9-diundecylbisthieno[2'',3'':4',5']thieno[2',3':4,5]pyrrolo[3,2-*e*:2',3'-*g*][2,1,3]benzothiadiazole-2, 10-diyl]bis[methylidene(5,6-difluoro-3-oxo-1H-indene-2,1(3H)-diylidene)]bis[propanedinitrile]]) bearing fluoride atoms activated by electron-withdrawing groups. One strategy that can be used to avoid these side reactions is using a protecting group for the thiol moiety.

Interestingly, some reports have indicated that S-acetyl-protected species can be used directly (i.e., without deprotection) to generate SAMs on gold and silver.^[21–23] Herein, we introduce two carbazole-based molecules with the thiol and thioacetate anchoring groups BrCzSH (2-(3,6-dibromo-9H-carbazol-9-yl)ethane-1-thiol) and BrCzSAC (S-(2-(3,6-dibromo-9H-carbazol-9-yl)ethyl)thioacetate), respectively (Figure 1a). These molecules were directly blended with the BHJ in solution prior to film coating. During post-thermal annealing of the completed devices with mild conditions, the molecules migrate within the active layer until reaching the interface between the active layer and silver electrode. There they form strong metal–sulfur interaction with silver atoms and self-assemble to form an optimal contact between the BHJ active layer and the silver electrode, and therefore enable hole transport to occur through the interface (Figure 1b).^[12,17,24] This process has been carefully optimized by varying the annealing temperature, annealing time, and additive concentration in the BHJ solution. This scalable strategy not only simplifies the device structure by suppressing the hole transporting layer (HTL) but can also improve the thermal stability and photostability of the solar cells.

2. Results and Discussion

2.1. Fabrication Process Optimization

Solution-processed single junction organic solar cells with an inverted architecture n-type-intrinsic-p-type (n-i-p) were fabricated and characterized. Control devices with the well-known evaporated MoO₃ interlayers were simultaneously fabricated as references. For the bulk heterojunction, PTQ10, a highly efficient polymer, showing a promising industrial scalability due to its simple structure,^[6,25] was used as a donor material. Y6, one of the best high-performance non-fullerene acceptor molecules (NFA),^[26] was used as an acceptor material. The device structure was ITO/ZnO (50 nm)/IC-SAM/BHJ (with or without BrCzSH or BrCzSAC) (100 nm)/(with or without) MoO₃ (7 nm)/Ag (80 nm). (See SI for more details) IC-SAM (IC-SAM: 4-((1,3-Dioxindan-2-ylidene)methyl)benzoic acid) has been used in previous studies to passivate the photocatalytic activities of

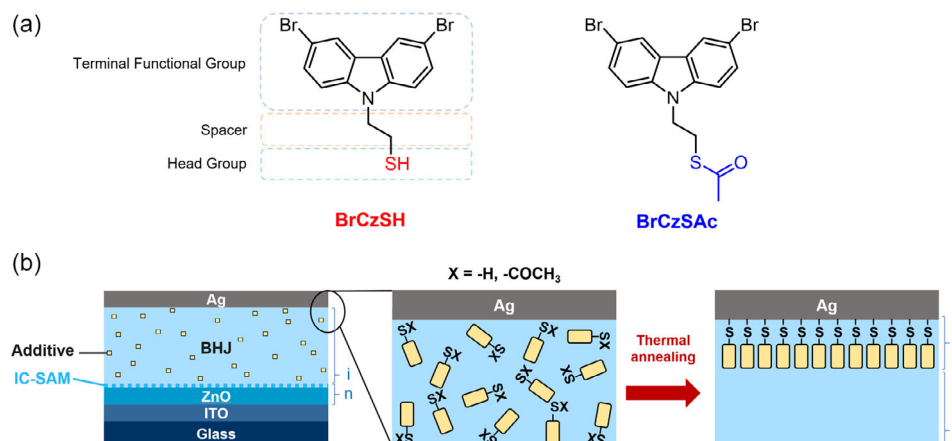


Figure 1. a) Chemical structures of BrCzSH and BrCzSAC molecules. b) Schematic representation of the general concept of this work. Molecules are blended into the bulk heterojunctions. Mild thermal annealing of the complete device after fabrication enables the migration of molecules toward the top electrode interface where they covalently bond to the silver electrode.

ZnO, to improve device stability, and has been shown to improve device performance.^[8,27,28] It was applied in the device architecture to ensure the inherent stability of control devices and to avoid any reactivity between ZnO and our molecules.

Devices without any HTL (ITO/ZnO/IC-SAM/BHJ/Ag) were also fabricated and characterized. As would be expected, they were virtually non-functional, with an average PCE of 0.12%. After thermal annealing for 10 min at 100 °C these devices exhibited an average PCE of 0.21%. This test was undertaken to demonstrate that the thermal annealing used in processing the SAM-modified devices has negligible effect when there is no HTL/SAMs in the device architecture (Table S1, Supporting Information). Control devices with MoO₃ exhibit an average PCE of 11.9%, which is typical for this architecture in our laboratory.

We investigated the performance of devices with BrCzSAC molecule in the BHJ before and after thermal annealing. Fresh devices, that are not thermally annealed, exhibited almost the same performance as the devices without HTL, with higher short-circuit current densities (J_{SC}) and open-circuit voltages (V_{OC}) (Table S1, Supporting Information). After thermal annealing at 100 °C for 10 min, the devices can exhibit significantly better device performances of 4.11%. From this result, we speculate that with the additional thermal energy imparted during the annealing process increases the diffusion mobility of the BrCzSAC and, by extension, BrCzSH molecules in the BHJ film. When the molecule's head moiety is oriented toward the silver electrode, a silver-sulfur bonding interaction occurs. This allows hole transportation in the devices and, as a consequence, higher charge transport can be measured during the device operation.

Moreover, a larger V_{OC} is measured, indicating improved energetic levels alignment at the interface between the active layer and the electrode. The origin of the increase in V_{OC} and the corresponding increase in device performance is confirmed by XPS measurements which identify the presence of a BrCzSH or BrCzSAC interlayer at the Ag/blend interface.^[29] This means the spontaneous formation of a BrCzSH or BrCzSAC accumulation at the interface acting as an organic/metal interlayer with hole-transporting ability. Despite this, a PCE of 4.11% is far from the reference devices indicating the process is still unoptimized at this point.

Consequently, the annealing temperature against the time were varied to investigate the progression of the device performance during the annealing process and to find the optimum annealing condition for further experiments. It was found that the optimum annealing temperatures of BrCzSH and BrCzSAC were 80 and 100 °C, respectively. Other conditions are displayed in Figure S19–S20, Supporting Information. As shown in **Figure 2**, for the first period of annealing, device performance showed significant improvement against the annealing time and after that became stabilized. This is due to the additive-metal interactions reducing the overall free energy of the system. One can suggest that when molecules bind to the silver surface, this forms a depletion zone near the surface, and over time simple entropy-driven random-walk diffusion leads to a net migration toward the surface. This diffusion process is terminated once full coverage of the metal surface is reached.^[30] The PCEs of the annealed devices exhibit a similar trend to the V_{OC} for both materials (Figure 2a,b). In addition, without annealing, BrCzSAC starts with only 1.2% of PCE compared

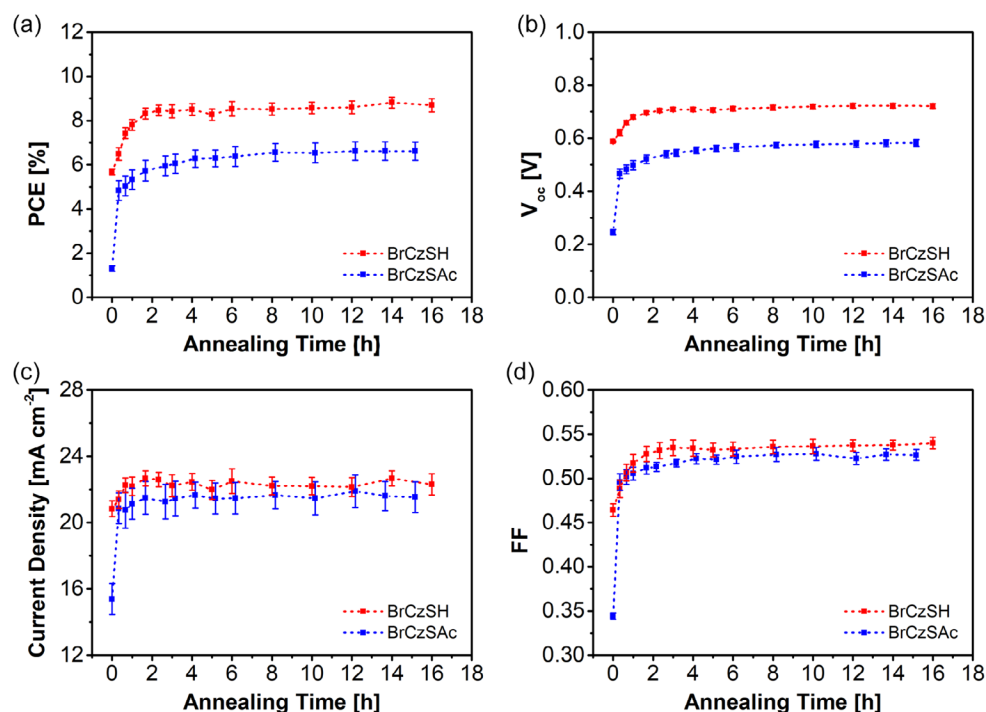


Figure 2. Device photoelectrical parameters corresponding to OPVs performance with an optimum annealing temperature of 80 °C for BrCzSH (bleu), and 100 °C for BrCzSAC (red) addition. a) PCE, b) V_{OC} , c) J_{SC} , and d) FF as a function of annealing time. Error bars indicate standard deviation on minimum eight cells.

to 5.7% with BrCzSH, which may speak to differences in the reactivity or mobility of the protected and unprotected thiols. After 20 min of heating and until stabilization, BrCzSAC and BrCzSH devices follow similar trends in PCE with 37% and 30% improvements. This enhancement occurs slowly, 8 h in the case of BrCzSAC and much less time, 6 h in the case of BrCzSH. This difference of speed underline once again a possible difference of reactivity or mobility of the two molecules. Another aspect is also that all parameters are improved (from 20 min annealing to stabilization), BrCzSAC device gained 21% of V_{OC} , 8% of FF, 4% of J_{SC} ; BrCzSH gained 14% of V_{OC} , 10% of FF, 5% of J_{SC} . All those parameter improvements confirm the interlayer formation, especially the V_{OC} , J_{SC} and FF gains suggest that better charge extraction is also achieved.

A series of OPV devices composed of PTQ10:Y6 blends with different BrCzSH and BrCzSAC concentrations were fabricated and characterized. As determined with previous experiments, devices were annealed at their optimal temperature 80 °C for 6 h with BrCzSH and 100 °C for 8 h for BrCzSAC devices. The photovoltaic parameters are presented in **Figure 3a–d** and Table S2 and S3, Supporting Information. When adding BrCzSH from 1 to 4 wt%, the device performance improved to around 59% of PCE (from 5.9% to 9.4%) and gradually dropped as the concentration increased, likewise showing the same tendency for V_{OC} . For BrCzSAC, the results showed that the PCE increased with increasing concentration from 4 to 24 wt%. After that, it dropped slightly at 28 wt% and significantly at 32 wt%. Moreover, there were similar trends in terms of V_{OC} and FF, but the optimum point was at the concentration of 28 and 20 wt%, with an average PCE of 8.09% and 8.17%, respectively. The J_{SC} trend appears consistent for every concentration

except 32 wt%. Interestingly, the J_{SC} remains steady when the BrCzSAC content increases from 4 wt% to 28 wt%. The external quantum efficiency (EQE) spectra confirmed these values, as shown in Figure S21b, Supporting Information.

The dipolar organic molecules of the additives provides a pathway to tune the barriers for charge-carrier injection into the active organic layer at the molecular scale by modifying the effective work function of the electrodes and thus adjusting the alignment of the metal Fermi level with the conduction states in the organic semiconductor.^[29,31] Therefore, adding BrCzSH and BrCzSAC in the BHJ can cause an increase in V_{OC} due to a shift of the silver cathode's work function by forming an interface. In addition, the highest achieved PCE on average was 9.4% for BrCzSH and 8.2% for BrCzSAC, with a very close FF of 0.55 and 0.56, respectively. This indicates the two additives have similar charge extraction properties when they form an interlayer between BHJ and silver electrode. Although the performances of devices with both additives were very close, they required a different amount of material to reach that performance (4 wt% for BrCzSH and 20 wt% for BrCzSAC). This can be rationalized by the different reactivities of thiol and thioacetate functional groups. Thiol is more reactive than the protected form as a thioacetate. That is the reason for using less material and a shorter annealing time for BrCzSH compared to BrCzSAC.

Moreover, **Figure 4a,b** displayed the current density–voltage (J – V) characteristics of optimized OPV devices with additives and a control device (ITO/ZnO/IC-SAM/BHJ)/MoO₃/Ag and their corresponding EQE spectra (photovoltaic characteristics are presented in **Table 1**). The devices exhibited broad EQE responses in the wavelength range of 300–1000 nm. Both conditions had similar photo-response behavior, in which PTQ10

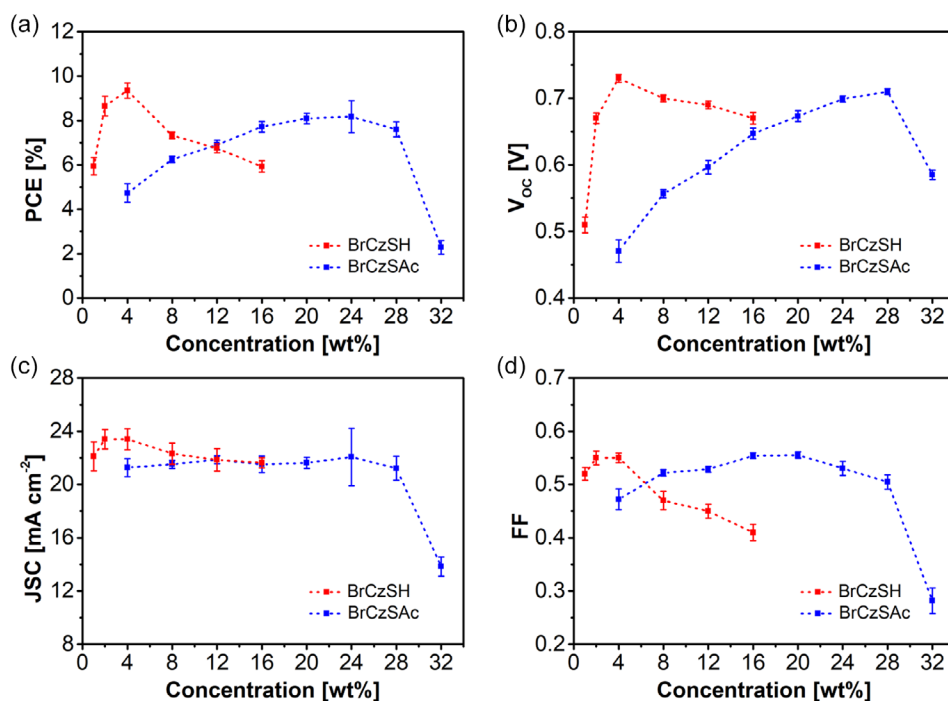


Figure 3. a) PCE, b) V_{OC} , c) J_{SC} , and d) FF as a function of different weight ratios of BrCzSH (bleu), and BrCzSAC (red) additive in PTQ10/Y6 BHJ. Error bars indicate standard deviation on minimum 8 cells.

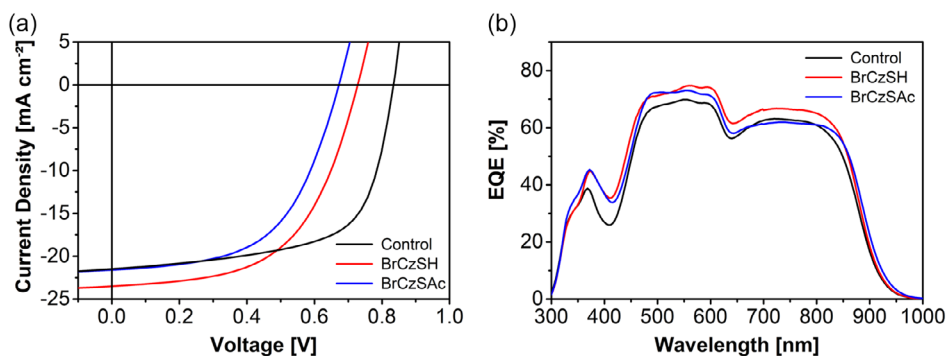


Figure 4. a) J - V curves of solar cells with the optimum annealing conditions, 80 °C for 6 h, and 100 °C for 8 h, for BrCzSH (red) and BrCzSAC (blue) additive respectively, compared to control device (black). b) Corresponding EQE spectra.

Table 1. Photovoltaic characteristics of optimized devices corresponding to OPVs performance with the optimum annealing condition of 80 °C for 6 h, and 100 °C for 8 h, for BrCzSH and BrCzSAC compared to MoO₃ HTL reference devices. The standard deviations are based on measurements of minimum eight cells.

Sample	J_{sc} [mA cm^{-2}]	V_{oc} [V]	FF	PCE [%]
Ref. with MoO ₃ as HTL	21.23 ± 0.41	0.83 ± 0.01	0.67 ± 0.01	11.90 ± 0.32
BHJ:4 wt% BrCzSH	23.40 ± 0.79	0.73 ± 0.01	0.55 ± 0.01	9.35 ± 0.35
BHJ:20 wt% BrCzSAC	21.63 ± 0.42	0.67 ± 0.01	0.56 ± 0.01	8.08 ± 0.23

contributed more than Y6, around 10%. These data indicate the addition of BrCzSH and BrCzSAC leads to the enhancement of EQE values, especially in the 380–650 nm range for both materials and all ranges for BrCzSH. This results in an improved J_{sc} when compared to the control device. The calculated integrated current densities are 19.3, 21.0, and 20.3 mA cm^{-2} (see Table S4, Supporting Information) for the control devices, with BrCzSH, and BrCzSAC, respectively. These results present the same trend, confirming the good agreement for interface formation due to the additives. Reflectance measurements were performed to understand the origin of those current density improvements (see Figure S22a, Supporting Information). In the spectral region between 350 and 550 nm, reflectance is higher for the control

device compared to the devices with additives, suggesting that optical effects in the devices with additives lead to substantial improvement of the EQE. In contrast, from 550 to 850 nm, there is no difference in the reflectance spectra between the different active layer, indicating that optical effect cannot explain the difference in the EQE spectra. Indeed, one can observe that differences in IQE (see Figure S22b, Supporting Information) appears to be the same than those noticed in EQE, signifying that an electronic phenomenon is driving the different improvement induced by the additives on this range of wavelength.

2.2. Material Properties and Physical Mechanisms

The details of the material synthesis and characterization of BrCzSH and BrCzSAC are provided in Figure S1–S17, Supporting Information. BrCzSH and BrCzSAC exhibit relatively good solubility in chloroform, a common solvent used for active layer ink formulations. They showed favorable thermal stability with a decomposition temperature (5% weight loss, T_{5d}) of 245 °C and 262 °C, respectively, observed by thermogravimetric analysis (Figure S22c, Supporting Information). The optical properties of each material (Figure S22d, Supporting Information) and polymer blends are compared using ultraviolet–visible (UV–Vis) absorbance (Figure 5a). PTQ10, a donor polymer, absorbs the light in the range of 300–650 nm, while the acceptor molecule Y6 absorbs in the range of

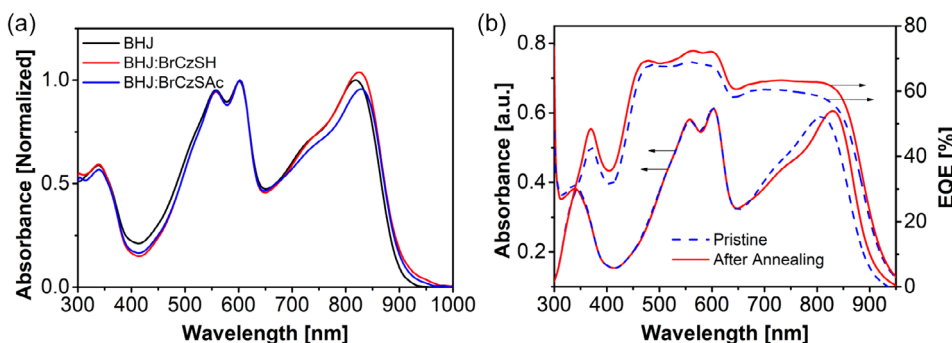


Figure 5. a) UV–Vis absorbance spectra in films of PTQ10:Y6 without (black) or with 8 wt% additives, BrCzSH (red) and BrCzSAC (blue). b) UV–Vis absorbance spectra of BHJ with BrCzSH additive before and after thermal annealing (6 h at 80 °C) compared to EQE spectra of OPV devices with BrCzSH additive before and after thermal annealing (6 h at 80 °C).

450–1000 nm. Our additive molecules, BrCzSH and BrCzSAC, exhibit almost the same absorbance profile with a weak absorbance in the range of 300–400 nm only. For each molecule, the blended BHJ films of PTQ10:Y6 with and without additives were investigated. The absorbance peak of PTQ10 is not significantly affected. Meanwhile, a slight bathochromic shift was observed for the Y6 absorbance peak (from 818 to 824 and 828 nm for BrCzSH and BrCzSAC addition respectively) in the BHJ with an additive when compared to bare BHJ.

To further understand the effect of thermal treatment, the UV–Vis spectra of BHJ:BrCzSAC blended before and after thermal annealing at 100 °C for 10 h were performed (Figure 6a). The results revealed that the absorbance of PTQ10 region was the same for both cases but different in Y6 region. The bathochromic shift, which is usually a sign of a *J*-stacking evolution. Zhu et al.^[32] demonstrate, among all studied parameters, that UV–Vis modification after annealing are signs of an increase of charge mobility generating an improvement of FF and J_{SC} and PCE. Those features in PTQ10:Y6 BHJ seems to be equivalent or more pronounced with the addition of V_{OC} improvement thanks to HTL interface creation. EQE spectra of the devices with BrCzSAC before and after annealing with the same conditions were investigated (Figure 6b). The annealed devices achieved progress of EQE in all range of spectra compared to before annealing and obtained an integrated current density of 20.80 and 19.62 mA cm⁻², respectively which confirms that the thermal annealing led to achieving a higher EQE value of devices.

In order to further demonstrate thiol bounding of molecules we carried out XPS measurements of silver substrates that were

soaked for 1 h in thiol (or thioacetate) solution. Some of them were just dried with compressed air and some of them were washed with the solvent. Comparison with pristine silver surface is presented Figure S24, Supporting Information. For experiment details see S.I. and for interpretation, see Figure S25 and S26, Supporting Information. An S 2p_{3/2} signal around 162.5 eV demonstrate bounding of the thiol. This observation is consistent with previous results reported by several research groups.^[33,34] The remaining S 2p_{3/2} around 163.7 eV shows unbound thiol attached to the surface. This last signal clearly decreases with the washing from 45% to 25% of the area, confirming the attribution. The same observation is noticeable with BrCzSAC, but here the unbound S 2p_{3/2} S–Ac signals are close to 163.6 eV with an equivalent loss of surface thanks to washing.

Vinokur et al. underline that the extent of migration and additive content at the organic–metal interface is governed by additive concentration, the strength of the driving force, and the diffusivity of the additive in the film. Thus, the driving force is correlated with the chemical affinity between additive–metal couple (sulfur–silver, in our case).^[30] Béthencourt et al. underline that the adsorption of the thioacetate moieties is less efficient or kinetically slower than that of the corresponding thiols.^[21]

To further demonstrate this mechanism in our devices, we used XPS to analyze the chemical composition of the organic–Ag interface of PTQ10:Y6:BrCzSH/BrCzSAC blends that were either not annealed or annealed after the Ag deposition. Devices were delaminated via tape exfoliation, allowing us to study internal silver–BHJ interface. See Figure S27, Supporting Information. In Figure 6a, a significant contribution

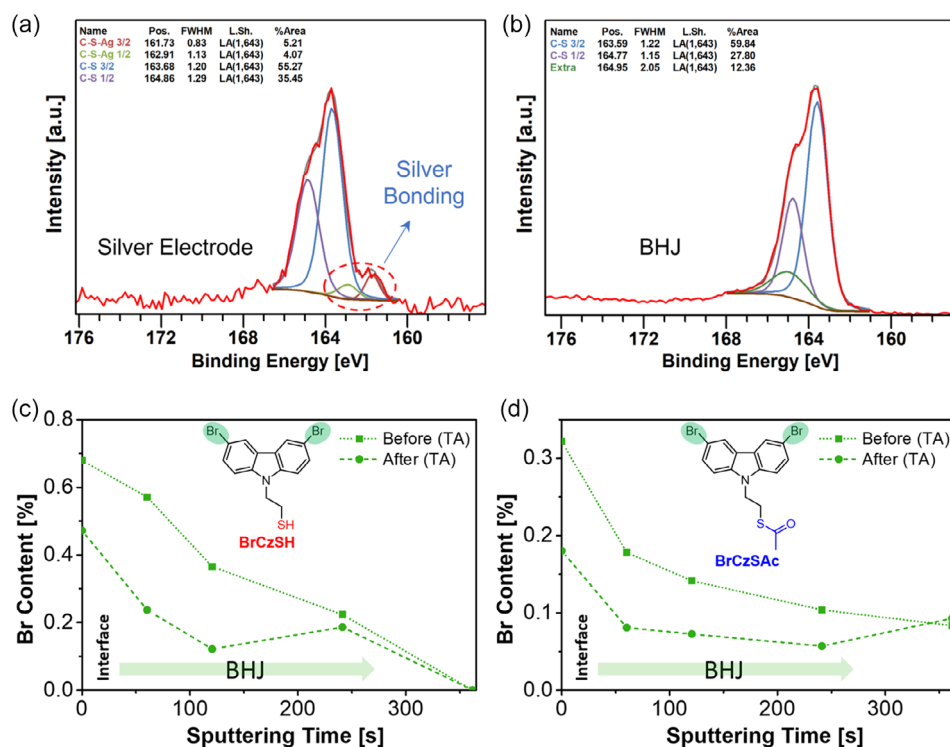


Figure 6. a,b) Analysis of OPV devices with thermal annealing where BrCzSAC were incorporated in BHJ. XPS S_{2p_{3/2}} emission spectrum (red line) observed at the silver electrode and in BHJ, respectively, back ground (brown line), cumulated fitted curves (gray line), and components (other colored lines). c,d) bromine content observed in BHJ layer with Ar sputter etching.

on the electrode interface can be attributed to thioacetate or thiol function around 164.0 eV but also to remaining traces of polymers and NFA.^[35] Furthermore, the S–Ag contribution at 162.0 eV provide evidence of the reaction of thiol with the electrode. Without the annealing, this contribution remains almost unchanged (Figure S28, Supporting Information), only a slight increase of S–Ag can be observed between these two analyses. The BHJ composition, see Figure 6b, shows also the same mix with thioacetate and thiophene belonging to polymer and NFA. No S–Ag signal are noticed. A third component that could be attributed to some oxidized sulfur due to handling that can be seen with signal around 165.0 eV.^[35] Similar observations were obtained when BrCzSH is added in the BHJ, as well on electrode as in BHJ. See Figure S29 and S30, Supporting Information.

Another important contribution when we probe deeper into the active layer (via etching with argon sputtering) is the distribution of bromine along the thickness, as this can be used to show the presence of BrCzSH or BrCzSAC. After annealing the bromine content decreases by around a factor of two (Figure 6c, d). This would follow from the accumulation of BrCzSH/BrCzSAC at the interface induced by annealing.

One of the key factors determining the driving force for charge extraction and hole transport through the active layer/Ag interface of inverted OPVs is the energy level alignment between the HTL and the active layer, which significantly affects the overall device performance.^[36,37] To have an insight of what is the impact of these molecules at the interface we performed Kelvin probe measurements of silver substrates modified by BrCzSH and BrCzSAC to investigate the work function (WF) of materials. The WFs of washed Ag/BrCzSH and Ag/BrCzSAC were determined to be -5.00 and -5.01 eV, respectively (Figure 7a). These values show that no matter which sulfur-containing group is used, an increase of Fermi level occurs, resulting in desirable HTL properties.

To confirm this aspect, UPS measurements were performed on the substrates. With the secondary electron cut off (SECO) (see Figure S31, Supporting Information) in kinetic energy we were able to directly obtain Fermi levels of 4.48, 4.60 and 4.70 eV for silver, Ag/BrCzSH and Ag/BrCzSAC, respectively. Here we had also an increase of almost 0.15 to 0.25 eV for BrCzSH and BrCzSAC, consistent with HTL properties but less impressive than the 0.3 eV observed with Kelvin probe.

Regarding the observed binding energy (plotted with respect to the Fermi level, Figure 7b), it can be observed that the HOMO of BrCzSH and BrCzSAC are at the same energy level. Additionally, as the coverage appears incomplete, the silver surface still provides enough states to align Fermi levels. Finally, as the onset of HOMO levels are at a BE of +1.1 eV we can reasonably advance that HOMO levels are at Silver Fermi level + Onset, which means -5.58 eV. This is in good accordance with cyclic voltammetry estimation of the PTQ10 HOMO of -5.54 eV.^[25]

If silver alone was donating electrons to PTQ10 to effect hole transfer, this would generate a certain loss of energy by stabilization (black bold arrow, Figure 7b). In the case of BrCzSH and BrCzSAC functionalization, the number of states between Fermi level to PTQ10 HOMO is almost divided by 2 (blue and red dash arrow). In contrast, BrCzSH and BrCzSAC, by their HOMOs provide a particularly adequate numbers of state to feel PTQ10 HOMO. This is even more noticeable for BrCzSH which can partially explain better performance with this additive. This gives us a general insight of mechanism those SAMs in OPV devices.

2.3. Device Stability

The thermal stability of devices was investigated under N_2 atmosphere, in the dark, at $85^\circ C$. Devices' photoelectrical parameters were measured before and after thermal annealing to compare the effect of temperature, as shown in Figure 8a. All device parameters were collected (Figure S32, Supporting Information) and the trends in normalized PCE are shown in Figure 8b.

After annealing at $85^\circ C$ for 100 h, both sets of devices with BrCzSH and BrCzSAC additives exhibited an improvement of PCE (10% for BrCzSH and 5% for BrCzSAC). While the control devices (ITO/ZnO/IC–SAM/BHJ/MoO₃/Ag) showed a reduction of 4% of PCE by losing V_{OC} and FF, which is partially compensated by an increase of J_{SC} . Thermal ageing of OPVs with MoO₃ is known and was reported by Chambon et al.,^[38] exhibiting diffusion of Mo in the active layer. The use of our approach revealed that the formation of an interface between BHJ and the electrode can help to maintain and may improve the thermal stability of organic solar cells.

To study photostability, another batch was exposed to light for up to 100 h (details in Supporting Information). The normalized PCE curves (Figure 8d) were calculated from all measured device

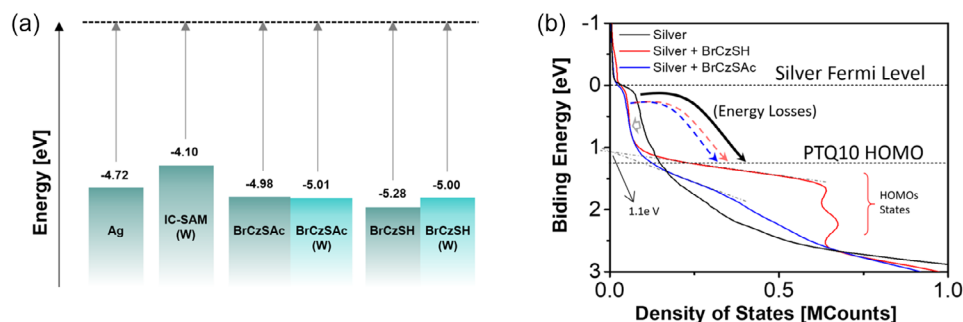


Figure 7. a) Energy level diagram of neat silver, IC-SAM over ZnO/ITO electrode and BrCzSH, BrCzSAC, over silver (washed (w) or not (measurements done in the air)). b) XPS measurements showing density of state of bare silver (black line) and silver treated by BrCzSAC (red line) or BrCzSH (blue line) thanks to Fermi levels alignment.

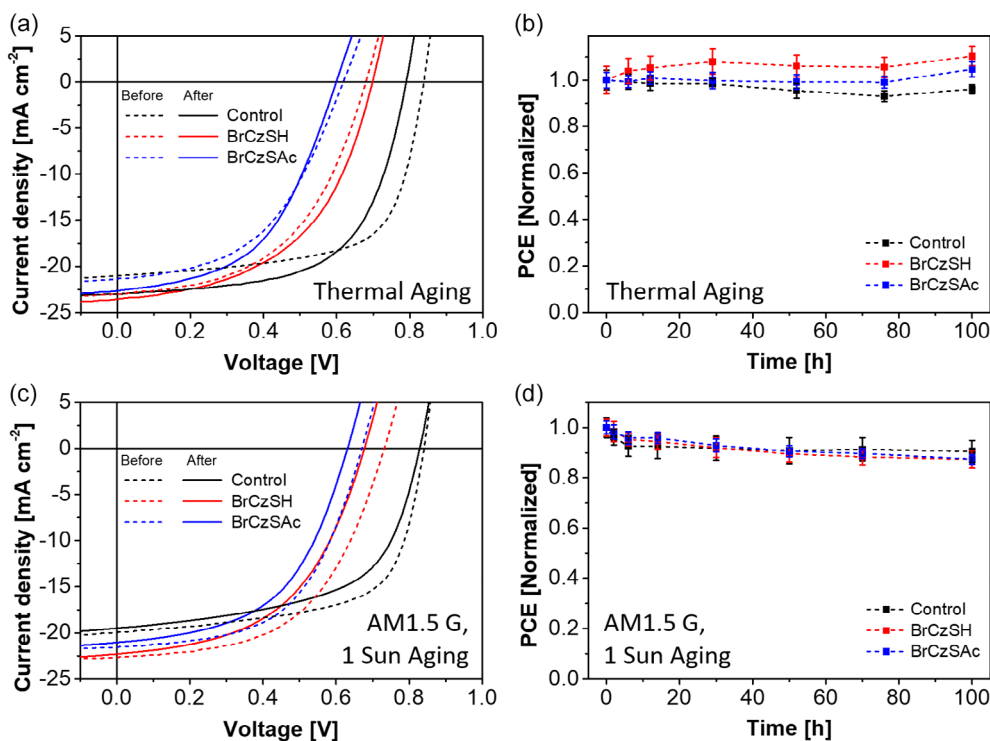


Figure 8. a) The characteristic $J-V$ curve of control device and optimized (thermally activated) devices with BrCzSH and BrCzSAC additive before thermal annealing (dash line) and after thermal annealing at 85 °C under N₂ atmosphere for 100 h (solid line). b) Corresponding normalized PCE as a function of annealing time. c) The characteristic $J-V$ curve of control device and optimized devices with BrCzSH and BrCzSAC additive before soaking under the light (dash line) and after under 1000 W m⁻² continuous light illumination at 50 °C in ambient air for 100 h (solid line). d) Corresponding normalized PCE as a function of soaking time. Error bars indicate standard deviation on minimum eight cells. Cells were kept at open-circuit voltage condition during aging.

parameters, as shown in Figure S33, Supporting Information. Devices with BrCzSH and BrCzSAC exhibited almost the same degradation behavior, a 13% reduction of PCE for both additives after 100 h of exposure. Moreover, even though control devices lose only 10% of PCE and seems to be stabilized, it was found that this was due to a continuous FF loss that was once again compensated by a recovery of J_{SC} after an initial burn-in (Figure S33d, Supporting Information). In contrast, devices with BrCzSH and BrCzSAC additives showed remarkably slow and uniform degradation, retaining over 80% of initial PCE after 100 h of light exposure, which is very encouraging for this proof of concept.

No significant degradation is observed in the devices with BrCzSH, contrary to what could be expected as depicted in the introduction. It can therefore be reasonably concluded that the thiol molecule did not chemically affect the molecules of PTQ10 and Y6. This observation can inform future additive design. Therefore, these data demonstrate that these new additive molecules can result in OPV devices with impressive thermal stability and favorable photostability, with potential for further development.

3. Conclusion

In order to contribute to the simplification of OPV industrial processing, we studied a proof of concept system where inverted

OPV devices presenting were fabricated without the need of an HTL. Molecules with HTL properties combined with SAM properties (BrCzSH and BrCzSAC) were introduced directly into the active layer during device fabrication. To activate the molecules, that is, induce migration to the top interface and binding to the silver electrode, mild thermal annealing was applied. Concentrations of 4 wt% for BrCzSH and 20 wt% for BrCzSAC were assessed to reach optimal performances. After thermal annealing of the completed devices for 6 h at 80 °C for BrCzSH and for 8 h at 100 °C for BrCzSAC, very encouraging PCEs of 9.4% and 8.2% were achieved, respectively. These features were confirmed by UPS analysis, showing silver-sulfur bonding and bromine repartition rearrangement sign of molecule migration. HTL properties were also investigated through Kelvin probe and UPS analysis, which confirmed the role played by these molecules as an HTL. Finally, thermal stability and photostability were investigated. Devices with additives present better thermal stability than control devices and the photostabilities were remarkably good with a retention of more than 80% of PCE even after 100 h of continuous light exposure. We demonstrated that the thiol functional groups introduced in the active layer did not significantly degrade either PTQ10 or Y6. This HTL-free concept is highly promising for the simplification of OPV solar modules at minimized manufacturing cost.

Supporting Information

Supporting Information is available from the Wiley Online Library or from the author.

Acknowledgements

The authors are warmly grateful to Dr. William Greenbank, assistant professor at University of Southern Denmark, and Dr. Sylvain Chambon, CNRS Researcher at University of Bordeaux, for proofreading.

Conflict of Interest

The authors declare no conflict of interest.

Author Contributions

Gilles Henri Roche: Conceptualization: (lead); Supervision: (lead); Writing—original draft: (supporting). **Suwapat Kongsabay:** Investigation: (lead); Writing—original draft: (lead). **Olivier Dautel:** Conceptualization: (supporting); Writing—original draft: (supporting); Writing—review and editing: (equal). **Vinich Promarak:** Supervision: (supporting); Writing—review and editing: (supporting). **Guillaume Wantz:** Funding acquisition: (lead); Supervision: (supporting); Writing—review and editing: (lead).

Data Availability Statement

The data that support the findings of this study are available from the corresponding author upon reasonable request.

Keywords

HTL, interface, OPV, stability, thiol

Received: July 30, 2024

Revised: August 27, 2024

Published online:

- [1] J. Fu, Q. Yang, P. Huang, S. Chung, K. Cho, Z. Kan, H. Liu, X. Lu, Y. Lang, H. Lai, F. He, P. W. K. Fong, S. Lu, Y. Yang, Z. Xiao, G. Li, *Nat. Commun.* **2024**, *15*, 1830.
- [2] L. Wang, C. Chen, Y. Fu, C. Guo, D. Li, J. Cheng, W. Sun, Z. Gan, Y. Sun, B. Zhou, C. Liu, D. Liu, W. Li, T. Wang, *Nat. Energy* **2024**, *9*, 208.
- [3] S. Guan, Y. Li, C. Xu, N. Yin, C. Xu, C. Wang, M. Wang, Y. Xu, Q. Chen, D. Wang, L. Zuo, H. Chen, *Adv. Mater.* **2024**, *36*, 2400342.
- [4] J. Fu, P. W. K. Fong, H. Liu, C. S. Huang, X. Lu, S. Lu, M. Abdelsamie, T. Kodalle, C. M. Sutter-Fella, Y. Yang, G. Li, *Nat. Commun.* **2023**, *14*, 1760.
- [5] K. Jiang, J. Zhang, C. Zhong, F. R. Lin, F. Qi, Q. Li, Z. Peng, W. Kaminsky, S. H. Jang, J. Yu, X. Deng, H. Hu, D. Shen, F. Gao, H. Ade, M. Xiao, C. Zhang, A. K. Y. Jen, *Nat. Energy* **2022**, *7*, 1076.
- [6] X. Kong, J. Zhang, L. Meng, C. Sun, X. Jiang, J. Zhang, C. Zhu, G. Sun, J. Li, X. Li, Z. Wei, Y. Li, *CCS Chem.* **2023**, *5*, 2945.
- [7] L. Zhu, M. Zhang, J. Xu, C. Li, J. Yan, G. Zhou, W. Zhong, T. Hao, J. Song, X. Xue, Z. Zhou, R. Zeng, H. Zhu, C. C. Chen, R. C. I. MacKenzie, Y. Zou, J. Nelson, Y. Zhang, Y. Sun, F. Liu, *Nat. Mater.* **2022**, *21*, 656.
- [8] Y. Li, X. Huang, K. Ding, H. K. M. Sheriff, L. Ye, H. Liu, C. Z. Li, H. Ade, S. R. Forrest, *Nat. Commun.* **2021**, *12*, 5419.
- [9] Y. Lin, Y. Firdaus, F. H. Isikgor, M. I. Nugraha, E. Yengel, G. T. Harrison, R. Hallani, A. El-Labban, H. Faber, C. Ma, X. Zheng, A. Subbiah, C. T. Howells, O. M. Bakr, I. McCulloch, S. De Wolf, L. Tsetseris, T. D. Anthopoulos, *ACS Energy Lett.* **2020**, *5*, 2935.
- [10] Y. Lin, Y. Zhang, J. Zhang, M. Marcinkas, T. Malinauskas, A. Magomedov, M. I. Nugraha, D. Kaltsas, D. R. Naphade, G. T. Harrison, A. El-Labban, S. Barlow, S. De Wolf, E. Wang, I. McCulloch, L. Tsetseris, V. Getautis, S. R. Marder, T. D. Anthopoulos, *Adv. Energy Mater.* **2022**, *12*, 2202503.
- [11] Y. Lin, A. Magomedov, Y. Firdaus, D. Kaltsas, A. El-Labban, H. Faber, D. R. Naphade, E. Yengel, X. Zheng, E. Yarali, N. Chaturvedi, K. Loganathan, D. Gkeka, S. H. AlShammari, O. M. Bakr, F. Laquai, L. Tsetseris, V. Getautis, T. D. Anthopoulos, *ChemSusChem* **2021**, *14*, 3569.
- [12] B. Shamieh, T. Sarkar, G. L. Frey, *J. Mater. Chem. C* **2020**, *8*, 8992.
- [13] Y. Lin, Y. Firdaus, F. H. Isikgor, E. Yengel, E. Faber, X. McCulloch, Y. Lin, L. Yu, Y. Xia, Y. Firdaus, S. Dong, C. Müller, O. Inganäs, F. Huang, T. D. Anthopoulos, F. Zhang, L. Hou, *Sol. RRL* **2019**, *3*, 1900179.
- [14] J. Yang, Y. Lin, W. Zheng, A. Liu, W. Cai, X. Yu, F. Zhang, Q. Liang, H. Wu, D. Qin, L. Hou, *ACS Appl. Mater. Interfaces* **2018**, *10*, 22485.
- [15] A. Al-Ashouri, A. Magomedov, M. Roß, M. Jošt, M. Talaikis, G. Chistiakova, T. Bertram, J. A. Márquez, E. Köhnen, E. Kasparavičius, S. Levenco, L. Gil-Escrig, C. J. Hages, R. Schlatmann, B. Rech, T. Malinauskas, T. Unold, C. A. Kaufmann, L. Korte, G. Niaura, V. Getautis, S. Albrecht, *Energy Environ. Sci.* **2019**, *12*, 3356.
- [16] T. Minamiki, Y. Ichikawa, R. Kurita, *Sensors* **2020**, *20*, 2228.
- [17] J. C. Love, L. A. Estroff, J. K. Kriebel, R. G. Nuzzo, G. M. Whitesides, *Chem. Rev.* **2005**, *105*, 1103.
- [18] Z. Wang, J. Chen, S. Oyola-Reynoso, M. Thuo, *Coatings* **2015**, *5*, 1034.
- [19] A. Ulman, *Chem. Rev.* **1996**, *96*, 1533.
- [20] C. Zeng, C. Liu, Y. Chen, N. L. Rosi, R. Jin, *J. Am. Chem. Soc.* **2016**, *138*, 8710.
- [21] M. I. Béthencourt, L. O. Srisombat, P. Chinwangso, T. R. Lee, *Langmuir* **2009**, *25*, 1265.
- [22] J. M. Tour, L. Jones II, D. L. Pearson, J. J. S. Lamba, T. P. Burgin, G. M. Whitesides, D. L. Aliara, A. N. Parikh, S. V. Atre, *J. Am. Chem. Soc.* **1995**, *117*, 9529.
- [23] A. J. Hallett, M. Broomfield, P. Christian, S. J. A. Pope, *Transit. Met. Chem.* **2014**, *39*, 195.
- [24] G. K. Jennings, P. E. Laibinis, *J. Am. Chem. Soc.* **1997**, *119*, 5208.
- [25] C. Sun, F. Pan, H. Bin, J. Zhang, L. Xue, B. Qiu, Z. Wei, Z. G. Zhang, Y. Li, *Nat. Commun.* **2018**, *9*, 743.
- [26] J. Yuan, Y. Zhang, L. Zhou, G. Zhang, H. L. Yip, T. K. Lau, X. Lu, C. Zhu, H. Peng, P. A. Johnson, M. Leclerc, Y. Cao, J. Ulanski, Y. Li, Y. Zou, *Joule* **2019**, *3*, 1140.
- [27] H. Liu, Z. X. Liu, S. Wang, J. Huang, H. Ju, Q. Chen, J. Yu, H. Chen, C. Z. Li, *Adv. Energy Mater.* **2019**, *9*, 1900887.
- [28] S. R. Forrest, F. Pan, H. Zhang, L. Xu, H. Li, Y. Li, C. Ji, Y. Qu, X. Huang, S. Hou, C. Z. Li, L. S. Liao, L. J. Guo, S. R. Forrest, *Adv. Mater.* **2019**, *31*, 1903173.
- [29] B. Shamieh, S. Obuchovsky, G. L. Frey, *J. Mater. Chem. C* **2016**, *4*, 1821.
- [30] J. Vinokur, I. Deckman, T. Sarkar, L. Nouzman, B. Shamieh, *Adv. Mater.* **2018**, *30*, 1706803.
- [31] G. Heimel, L. Rومانer, E. Zojer, J. L. Bredas, *Acc. Chem. Res.* **2008**, *41*, 721.
- [32] W. Zhu, A. P. Spencer, S. Mukherjee, J. M. Alzola, V. K. Sangwan, S. H. Amsterdam, S. M. Swick, L. O. Jones, M. C. Heiber,

- A. A. Herzing, G. Li, C. L. Stern, D. M. DeLongchamp, K. L. Kohlstedt, M. C. Hersam, G. C. Schatz, M. R. Wasielewski, L. X. Chen, A. Facchetti, T. J. Marks, *J. Am. Chem. Soc.* **2020**, *142*, 14532.
- [33] D. G. Castner, K. Hinds, D. W. Grainger, *Langmuir* **1996**, *12*, 5083.
- [34] G. H. Roche, D. Thuau, P. Valvin, S. Clevers, T. Tjoutis, S. Chambon, D. Flot, Y. H. Geerts, J. J. E. Moreau, G. Wantz, O. J. Dautel, *Adv. Electron. Mater.* **2017**, *3*, 700218.
- [35] G. M. Paternò, V. Robbiano, K. J. Fraser, C. Frost, V. García Sakai, F. Cacialli, *Sci. Rep.* **2017**, *7*, 41013.
- [36] S. Wang, T. Sakurai, W. Wen, Y. Qi, *Adv. Mater. Interfaces* **2018**, *5*, 1800260.
- [37] S. Wang, T. Sakurai, W. Wen, Y. Qi, *Adv. Mater. Interfaces* **2020**, *7*, 2000423.
- [38] S. Chambon, L. Derue, M. Lahaye, B. Pavageau, L. Hirsch, G. Wantz, *Materials* **2012**, *5*, 2521.